Neutron-scattering studies of an electron-irradiated ^{62}Ni–41.4-at.%-^{65}Cu alloy

W. Wagner, R. Poerschke, and A. Axmann
Hahn-Meitner-Institut für Kernforschung Berlin GmbH, Glienicker Strasse 100, D-1000 Berlin 39, Germany

D. Schwahn
Institut für Festkörperforschung der Kernforschungsanlage Jülich, D-5170 Jülich, Germany
(Received 11 October 1979)

Neutron-diffraction studies of the null matrix ^{62}Ni–41.4-at.%-^{65}Cu have been performed after thermal treatment and after irradiation with 3-MeV electrons at temperatures between 373 and 510 K. The diffuse neutron scattering has been measured to determine the Warren-Cowley short-range-order parameters and additionally the neutron small-angle scattering has been investigated for detecting any possible decomposition or segregation in the Ni-Cu alloy. In the special case of Ni-Cu alloys the experiments demonstrate the successful combination of electron-irradiation and neutron-diffraction measurement, two experimental procedures with normally contradictory requirements. As a result of the diffuse scattering a significant increase of the atomic short-range clustering under irradiation has been observed, corroborating the interpretation of previous electrical-resistivity and magnetic-susceptibility measurements. In small-angle scattering the formation of periodic concentration fluctuations is observed as it is expected for spinodal decomposition, giving the first experimental evidence of the suggested miscibility gap in Ni-Cu.

I. INTRODUCTION

For Ni-Cu alloys the earlier suggested short-range clustering[1-16] was established by diffuse-neutron-scattering investigations.[17-21] By using the data on short-range clustering, Vrijen and Radelaar[21] calculated the shape and location of a miscibility gap with the result that the maximum should be located at 65-at.% Ni in a temperature range between 360 and 600 K. The experimental proof of the miscibility gap in Ni-Cu is still missing for the reason that the lowest annealing temperature leading to an observable change of the atomic distribution in reasonable annealing times is about 620 K.[6]

Although the temperature region below 620 K is inaccessible for thermal diffusion, a remarkable atomic mobility leading to decomposition can be expected during particle irradiation. This mobility is due to the migration of radiation-induced defects which have been found to cause interdiffusion even at low temperatures, for interstitials down to about 100 K.[12-16]

In the present work 3-MeV electron irradiation has been applied in order to achieve sufficient atomic mobility below 620 K. With this type of irradiation, the energy transferred by the electron to a lattice atom is so low that most of the defects are produced in single displacement processes, providing a statistical defect distribution, a good prerequisite for homogeneous radiation-enhanced diffusion.

The change in atomic distribution of the alloy components due to irradiation has been investigated by means of neutron scattering: diffuse neutron scattering (DNS) for determining the Warren-Cowley short-range-order (SRO) parameters, and complementary to the diffuse scattering, small-angle scattering (SAS) for detection of the expected decomposition or any possible segregation.

For reasons outlined in detail later, electron irradiation and neutron diffraction are two experimental procedures with contradictory requirements. For a successful application of diffuse neutron diffraction to specimens suitable for electron irradiation, some special experimental conditions had to be fulfilled, primarily the use of isotopically enriched specimen material ("null matrix") and optimum experimental conditions for scattering-data collection, especially the use of a multidetector diffractometer for the collection of the diffuse-scattering data. Because of the importance of the experimental conditions for a successful realization of our experiment, the present paper predominantly gives an essential description of the experimental details. Furthermore, the DNS and SAS measurements after thermal treatment and after irradiation at temperatures between 373 and 510 K are given. Detailed conclusions both on the short-range-clustering data and on the SAS data with respect to phase stability will be presented elsewhere.[22,23]

II. EXPERIMENTAL

A. Electron-irradiation conditions

The radiation-enhanced diffusion coefficient in metals and alloys was proved to hinge upon the mobility and concentration of excess point defects,

e.g., vacancies and interstitials.[24] The mobility of each defect species depends on the migration enthalpy by an Arrhenius law, i.e., it depends on the local specimen temperature. Hence, one of the principal irradiation conditions is a uniform specimen temperature during irradiation. Moreover, the defect concentration is proportional to the local defect production rate; hence, the second prerequisite for proper irradiation conditions is a homogeneous defect production rate in the whole specimen volume.

Even if the beam current density is uniform over the specimen area, the homogeneity of defect production is impaired by two physical effects:

(1) By scattering processes, the electrons are deviated from their incident direction, which leads to an extension of their effective path length.[25] As a consequence, the defect production rate per unit of specimen thickness increases with increasing penetration depth. The quantitative treatment of this effect yields the following formula for the path extension[26]:

$$\Delta s = 215\left(\frac{1+1/a}{2+a}\right)^2 \frac{s^2}{L}\,, \tag{1}$$

with

$$L^{-1} = 0.0292 r_0 Z(Z+1)\Omega^{-1}\ln(183/Z^{1/3})\,,$$

and where s is the penetration depth into the sample in the incident-beam direction, a is the electron energy in units of the rest energy, Z is the atomic number, r_0 the electron radius, and Ω the atomic volume.

(2) Owing to collisions in the material, the electron energy decreases continuously with increasing distance from the incidence surface. As a consequence, a continuously decreasing defect production rate with increasing penetration distance is obtained.

For quantitative treatment we calculate the displacement cross section $\sigma_d(x)$ at a penetration distance x (where $x = s + \Delta s$) given by the formula

$$\sigma_d(x) = \sigma_d(x=0) - (d\sigma_d/dE)(dE/dx)x\,, \tag{2}$$

where $\sigma_d(x=0)$ is the displacement cross section at the incidence surface which the electrons hit with primary energy E_0. In Ni-Cu there is a nearly constant electron energy loss $dE/dx = 1.22 \pm 0.40$ MeV/mm for electron energies between 0.5 and 3.0 MeV.[27] With regard to the energy dependence of σ_d, it was found as an empirical result for pure Cu and concentrated Cu-Zn alloys that σ_d approximately obeys a logarithmic E dependence[28] for energies above the threshold energy. Taking this same energy dependence into account, we have calculated the effective displacement cross section in Ni-Cu according to Eq. (2) for electron irradiation with an incident energy of 3 MeV. The results are shown in Fig. 1 as a function of penetration depth, together with the result for each effect alone.

For short penetration distances both effects nearly compensate each other. For 3-MeV irradiation of our alloy, the effective defect production rate increases by about 10% at a depth of 0.50 mm which is the maximum thickness of our samples. The inhomogeneity of the production rate can be reduced by a factor of 2 by alternating irradiations, exchanging the front and back of the sample with respect to the beam direction. The irradiation was carried out at the 3-MeV Van de Graaff accelerator of the Physikalisch-Technische Bundesanstalt, Berlin. The electrons are guided in an evacuated beam tube by a set of water-cooled Cu diaphragms carefully aligned with the sample area to be irradiated. The irradiation device is shown in Fig. 2. The beam from the accelerator has a Gaussian intensity profile with a half width of about 4 mm. To ensure a homogeneous illumination of the total sample area of about 1.5×3.5 cm^2, the beam is scanned periodically by horizontal and vertical magnetic fields produced by two pairs of Helmholtz coils which are supplied by a current-controlled triangular generator (vertical frequency 36 Hz, horizontal frequency 1000 Hz). Before each irradiation run, the profile of the scanned beam has been measured in the Faraday cup, F_1, behind the water-cooled diaphragm B_1 (diameter: 0.30 ± 0.02 mm) which is also used as a shutter to interrupt the irradiation after a given dose. The scanning amplitude was adjusted to produce a beam

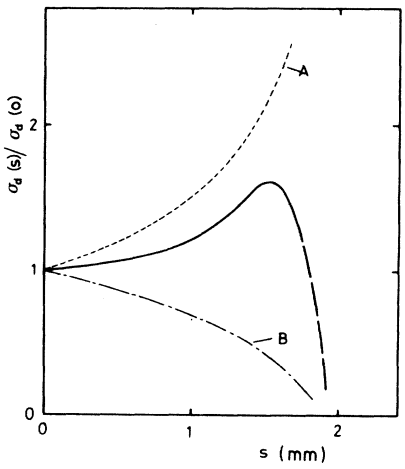

FIG. 1 Calculated effective displacement cross section in Ni-Cu for 3-MeV electron irradiation as a function of penetration depth s. In addition the effect of path extension only A and the effect of energy loss only B are given.

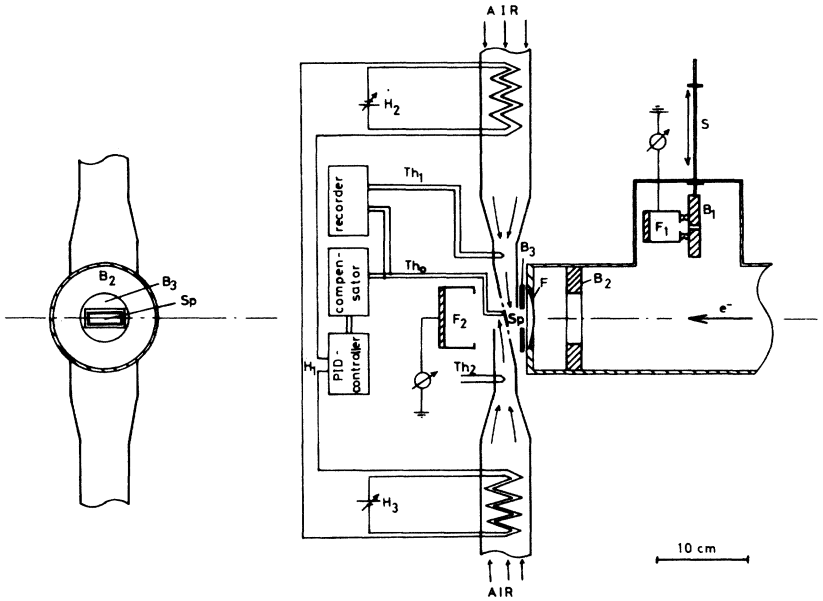

FIG. 2 Irradiation device. Right: sectional view of the beam tube and the irradiation device with a schematical sketch of the temperature control. Left: view of diaphragms and specimen from the accelerator. B_1, B_2, B_3, Diaphragms; F, Stainless-steel foil; F_1, F_2, Faraday cups; H_1, H_2, H_3, Heaters; S, Shutter; Sp, Specimen; Th_1, Th_2, Th_3, Thermocouples.

homogeneity of better than 5% over the sample area.

During irradiation the electron beam is measured in the Faraday cup, F_2, behind the specimen (Sp). The total electron dose is determined by time integration of the Faraday-cup current. The flux density is given by the Faraday-cup current divided by the area of diaphragm B_3. Within an accuracy of 5% the flux density determined by this method is in good accordance with the flux density measured with diaphragm B_1 and Faraday cup F_1.

The electrons penetrate a 20-μm stainless-steel foil (F) at the end of the beam tube and then reach the air-cooled specimen. By passing through the specimen, the energy loss of the electrons causes a heating of the specimen during irradiation. For cooling and for maintaining a given irradiation temperature, the sample was subjected to a forced air current, preheated by a heater H_1. Continuous registration of the sample temperature, which was measured by a Cu-constantan thermocouple (Th_0), and of the air temperature before passing by the sample, was made with thermocouples Th_1 and Th_2. The desired temperature was maintained by a PID (proportional integral differential) controller. In addition, constant heat power was fed to heaters H_2 and H_3 to extend the temperature range. By this arrangement the specimen temperature could be kept constant during irradiation within a limit of ±1 K.

Before carrying out the alloy irradiation, the temperature increase of the specimen, i.e., the difference between specimen temperature and air temperature ($T_{Sp} - T_a$) was measured at five different locations on the sample area of a dummy sample. The average T increase between different thermocouple positions is given in Table I for two different specimen thicknesses and electron flux densities. The maximum T deviation between different thermocouple positions, due to different coupling between sample and thermocouples, was on the order of 10% of the T increase. This yields an error of the same order of magnitude of the specimen temperature. The specimen thickness and beam current density were limited to values which yield a maximum temperature increase of

TABLE I. Average temperature increase ($T_{Sp} - T_a$) of the specimen during irradiation for two different specimen thicknesses (d) and electron flux densities (i).

d (mm)	i (10^{-6} A/cm^2)	$T_{Sp} - T_a$ (K)
0.500	6	70
0.500	12	140
0.200	6	30
0.200	12	55

about 60 K, and a maximum temperature error of 6 K.

B. Neutron diffraction

1. Introduction

The differential cross section for elastic scattering of thermal neutrons from a binary AB alloy arises mainly from two contributions: first Bragg scattering, given by[29]

$$\left.\frac{d\sigma}{d\Omega}\right|_B = (c_A b_A + c_B b_B)^2 \sum_n \sum_m e^{i\vec{\kappa}(\vec{r}_n - \vec{r}_m)}, \tag{3}$$

and second, order-disorder scattering which is given by[29]

$$\left.\frac{d\sigma}{d\Omega}\right|_D = \sum_n \sum_m [b^n b^m - (c_A b_A + c_B b_B)^2] e^{i\vec{\kappa}(\vec{r}_n - \vec{r}_m)}; \tag{4}$$

c_A and c_B are the atomic fractions of the components A and B, b_A and b_B are their effective scattering lengths, b^n and b^m are the scattering lengths at the lattice sites n and m, respectively, and $\vec{r}_n$ and $\vec{r}_m$ are the corresponding position vectors. $\vec{\kappa}$ is the scattering vector.

In the absence of long-range interaction effects, Eq. (4) reduces to diffuse short-range-order scattering which for polycrystalline cubic alloys becomes

$$\left.\frac{d\sigma}{d\Omega}\right|_{SRO} = N c_A c_B (b_A - b_B)^2 \left(1 + \sum_{i=1}^{\infty} z_i \alpha_i \frac{\sin \kappa r_i}{\kappa r_i}\right), \tag{5}$$

where α_i is the Warren-Cowley SRO parameter of shell i and z_i the corresponding coordination number. N is the number of lattice sites of the system.

For simplicity the Debye-Waller factor and the other contributions to the differential scattering cross section, e.g., size-effect scattering, isotopic incoherence, spin incoherence, and multiple scattering have been omitted in Eq. (5). Their contributions will be discussed later in detail.

To investigate order-disorder effects for reasons of optimal intensity rates, the scattering intensity factor $(b_A - b_B)^2$ in Eq. (5) should be as large as possible, especially if the size of the specimen is limited by other experimental conditions, in our case electron irradiation. By use of the isotopes ^{62}Ni, which has a negative scattering length ($b_{^{62}\mathrm{Ni}} = -0.87 \times 10^{-12}$ cm) and ^{65}Cu ($b_{^{65}\mathrm{Cu}} = +1.11 \times 10^{-12}$ cm), the scattering difference increases drastically in comparison to an alloy composed of natural Ni ($b_{\mathrm{Ni}} = 1.03 \times 10^{-12}$ cm) and Cu ($b_{\mathrm{Cu}} = 0.76 \times 10^{-12}$ cm). The enhancement reaches a factor of about 40 in the middle of the composition range. Simultaneously with the increase of order-disorder scattering, the cross section for Bragg scattering, given by the factor $(c_A b_A + c_B b_B)^2$, decreases. For a certain concentration, in our case $^{62}\mathrm{Ni}_{0.586} - {}^{65}\mathrm{Cu}_{0.414}$, it vanishes completely. This so-called "null matrix" or "null Bragg alloy" was used in our experiment.

2. Technical device for diffuse-scattering measurements

All neutron-diffraction-data measurements were carried out at room temperature. The diffuse scattering was measured with a diffractometer equipped with a multidetector at the reactor BER II, Berlin.[30] The schematic experimental device is given in Fig. 3(a). The thermal reactor neu-

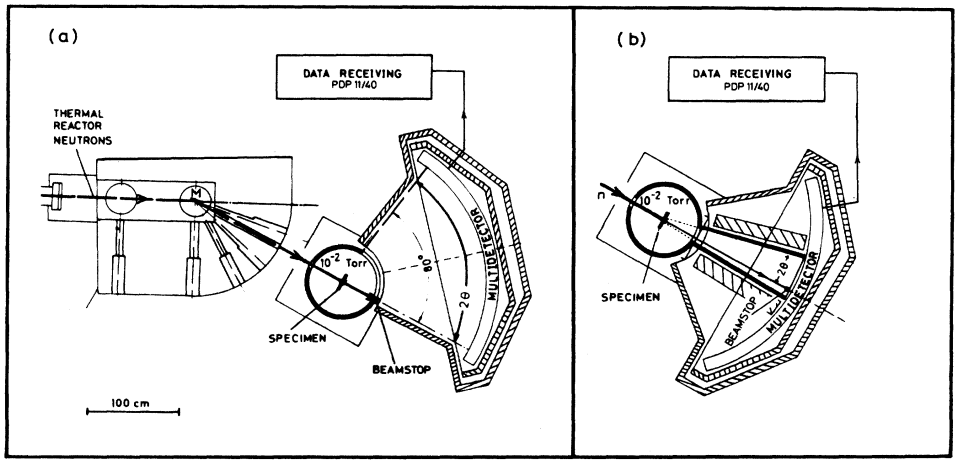

FIG. 3. Schematic experimental device for the neutron-diffraction measurement at the BER II. (a) Diffuse SRO-scattering measurement. (b) SAS measurement.

trons were monochromized by reflection at a monochromator crystal (M). To obtain the wavelength of 2.40 Å, a graphite monochromator was used with an additional graphite filter to restrict higher-order neutrons. A second, shorter wavelength (1.23 Å) was obtained by reflection at the (311) plane of a Ge single-crystal monochromator where no second-order reflection occurs.

The minimum collimation of the beam tube is about 2°, corresponding to a wavelength spread of $\Delta\lambda/\lambda \approx 0.05$. This has been accepted to be adquate for the diffuse-intensity measurements of our experiment; every additional collimation would have led to a loss of intensity. The scattered intensity was collected in a multidetector which contains 400 parallel proportional counters. They are positioned on an 80°-circle sector with a radius of 150 cm in a BF_3-filled chamber. The specimen is positioned at the center of the circle. By this arrangement the horizontal angular resolution is 0.2°, or 0.0035 rad, and the vertical-slit height of 10 cm leads to a vertical angular resolution of 0.0667 rad. For a detailed description of the multidetector see Ref. 31.

The minimum angle which could be detected under normal conditions for diffuse data collecting was about 4.5°; below this angle the background from the primary beam increases steeply. (By the use of special equipment and the slit arrangement which is described below, smaller minimum angles were obtained). The intensity is measured simultaneously over an angular range of $4.5° \leq 2\theta \leq 84.5°$ which corresponds to a scattering-vector range of $0.206 \leq \kappa\ (\text{Å}^{-1}) \leq 3.52$ for 2.40-Å neutrons and $0.400 \leq \kappa\ (\text{Å}^{-1}) \leq 6.87$ for 1.23-Å neutrons. Using these two wavelengths a diffuse κ range of $0.206 \leq \kappa\ (\text{Å}^{-1}) \leq 6.87$ was covered.

Without sample the background was nearly isotropic, except for the close vicinity of the primary beam. Its intensity could be held below one count per minute and channel by evacuating the specimen area and mounting screening walls of boron paraffin and cadmium around the detector. By use of an automatic specimen-exchange device, the intensity was measured in several alternating runs of one or two hours, once with the specimen in the beam and once without. In this way, long-time drifts of the background could be perceived and corrected, and the reproducibility of the measurement could be tested.

For calibration of the neutron wavelength and the scattering angle a standard Al_2O_3 powder was used. Incoherent scattering of vanadium was used for absolute calibration of the measured intensity, and moreover to correct for asymmetric diaphragms and screening absorption effects which were significant, especially at the sides of the multidetector. Fluctuations of the primary-beam intensity were permanently controlled by the use of a monitor detector.

The variation of the detecting cross section for the 400 different positions is of the order of only 1.3%, showing a statistical distribution. Therefore, correction of the counting rates with respect to the detector acceptance as a rule was not necessary and was omitted. Only for measurements with smaller statistical half width this correction was made using the incoherent scattering of vanadium.

3. *Small-angle scattering*

For extending the covered κ range to values below 0.20 Å^{-1}, the small-angle-scattering facility at the FRJ-2 reactor of the KFA Jülich was used. For detailed description of the apparatus see Schelten.[32,33] The detector was positioned at distances of 3 and 1 m from the specimen recording a κ range of $0.01\ \text{Å}^{-1} \leq \kappa \leq 0.06\ \text{Å}^{-1}$, respectively, $0.04\ \text{Å}^{-1} \leq \kappa \leq 0.22\ \text{Å}^{-1}$, by using a neutron wavelength of 7.2 Å. Together with diffuse scattering, the diffraction spectra were observed over a range of nearly three orders of magnitude in the scattering vector, for $\kappa = 0.01\ \text{Å}^{-1}$ to $\kappa = 7.0\ \text{Å}^{-1}$.

For correction of the detector acceptance and for calibration of the small-angle intensity, and incoherent scatter (Lupolen), calibrated with a vanadium standard, was used.

In addition to the SAS measurements performed at Jülich, SAS measurements were performed at the BER II. Here special equipment was constructed for measuring at small scattering angles also with the multicounter diffractometer [see Fig. 3(b)]. By means of a vacuum chamber with a channel reaching close to the window of the multidetector the whole flight path of the neutrons from the specimen to the detector could be evacuated. Preventing air scattering by this device the primary beam divergence could be limited to the geometric width given by the collimation. By using a special arrangement of graduated cadmium and boronparaffin diaphragms and screening, the minimum angle reached with an acceptable intensity to background ratio (≈1) was about 0.6°. The cross section of the vacuum channel of 100×300 mm^2 at the end is reduced by a 30-μm stainless-steel foil. The width of 300 mm together with a minimum scattering angle of 0.6° gives the covered κ range, by using 2.4-Å neutrons, as $0.03\ \text{Å}^{-1} \leq \kappa \leq 0.50\ \text{Å}^{-1}$.

C. Specimen preparation

To meet the experimental requirements described above, the specimens with foil geometry (area: about 37×15 mm^2) and a thickness of 0.2

and 0.5 mm were used. The used isotopically enriched Cu was purchased from Oak Ridge National Laboratories, the Ni from the U.S.S.R. by Isotron GmbH, Berlin. The corresponding concentrations and scattering lengths are given in Table II, the main impurities in Table III. The Cu material which was received as oxide was reduced during a 19-h annealing at 1070 K within flowing hydrogen. After mixing Cu and Ni in the atomic proportion 41.4 : 58.6, which corresponds to the concentration of the null matrix, the material was melted twice in an Al_2O_3 crucible in a high-frequency induction furnace and rapidly cooled. To obtain the necessary heat-conducting atmosphere for fast cooling and to limit the evaporation of Cu, the furnace tube was filled with 750 Torr argon of high purity. The ingot was pressed to a thickness of about 4 mm, and after a further reduction treatment in flowing H_2 at 1070 K, it was brought to a thickness of 0.50 mm by cold rolling in various directions and subsequently homogenized by a 24-h annealing at 1300 K. Then the sample was cut into three pieces of nearly the same mass, and two of them were rolled to a final thickness of 0.200 mm, and 0.180 mm, respectively. Thereafter all three samples were homogenized for 48 h at 1070 K. Finally, to achieve a uniform and distinct atomic distribution as initial state before irradiation, the three samples were annealed for 6 h at 870 K and furnace cooled with a low cooling rate (48 h from 870 to 300 K) to avoid quenching of excess vacancies.

The composition of the sample was checked by an x-ray analysis of the lattice constant which gave a value of $a_0 = 3.5574 \pm 0.0002)$ Å at 299 K, corresponding to a concentration of (58.5 ± 0.5)-at.% Ni.[34] The neutron scattering in the vicinity of the Bragg positions, even with a statistical error of less than 0.2%, did not show any indication of Bragg reflections (see Fig. 4). A chemical analysis yielded the impurity concentrations listed in Table III. An additional secondary-ion mass-spectroscopy (SIMS) analysis showed that the specimen did not contain other impurities of significant concentration.

The specimens were mechanically clamped to a frame-shaped stainless-steel specimen holder. Since in addition to the neutron scattering the SRO state has been controlled by electrical-resistivity measurements to enable a comparison with the data in the literature,[12-16] constantan wires to supply current and measure the potential were spot welded to the edges of the specimen. In addition, a Cu-constantan thermocouple was attached to the edge of the specimen to control the specimen temperature during irradiation. Electrical isolation was achieved by two mica foils between the specimen and the steel frame. For neutron scattering, all extraneous materials could easily be shielded with a cadmium mask without losing more than 2 mm of the specimen length.

D. Data handling

For the data reduction anumber of corrections must be made: The measured background is subtracted, taking into account the fact that the part of the background coming from the primary beam is affected by the specimen absorption, and the intensity is corrected for geometric effects and absorption. As discussed by Warren,[29] the thermal vibrations of the lattice were accounted for

TABLE II. Concentration and scattering lengths of the used isotopically enriched specimen material and scattering lengths of natural Cu and Ni.

Material	Concentration (at.%)	Scattering length (10^{-12} cm)
^{58}Ni	2.00	1.480 ± 0.008
^{60}Ni	1.17	0.282 ± 0.002
^{61}Ni	0.35	0.760 ± 0.006
^{62}Ni	96.30 ± 0.30	−0.850 ± 0.020
^{64}Ni	0.18	−0.037 ± 0.007
^{63}Cu	0.30	0.672 ± 0.015
^{65}Cu	99.70	1.110 ± 0.020
Ni (nat)		1.030 ± 0.010
Cu (nat)		0.763 ± 0.004

TABLE III. Main impurities of the used specimen material.

Chemical impurity	Concentration (at.%) Cu[a]	Ni[a]	Ni − Cu
Ag	< 0.01		0.0004[b]
Al	< 0.03	< 0.0009	
Bi	< 0.02	< 0.001	
Cd	< 0.05	< 0.001	
Cc	< 0.05	< 0.006	
Cr	< 0.05	< 0.001	<0.0002[c]
Fe	≤ 0.01	< 0.003	0.0045 ± 0.005[c]
Si	0.01	0.002	
Mn	< 0.01	< 0.0008	
Mo	< 0.02	< 0.0003	
Pb	< 0.02	< 0.001	
Pt	< 0.05		0.0090[b]
Sn	< 0.02	< 0.001	
Zn	< 0.2	0.007	
alkali and alkaline earth	< 0.05	<0.024	

[a] Furnisher analysis.
[b] Activation analysis.
[c] Chemical analysis.

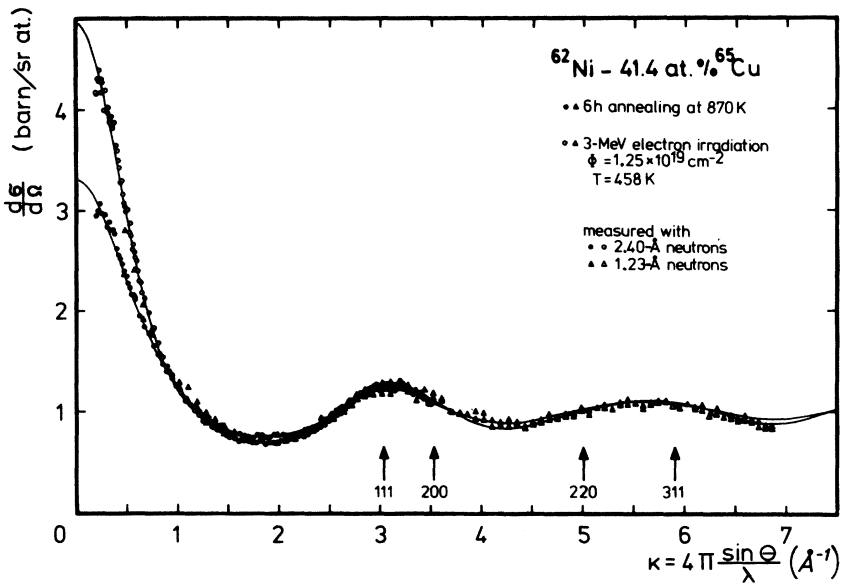

FIG. 4. Typical diffuse SRO-scattering patterns, measured at the multidetector diffractometer at BER II. The data have been corrected only for thermal background and geometric effects in transmission. The solid lines are the least-squares fits of Eq (2.3) to the experimental data.

by taking the mean square amplitudes of these vibrations and considering the effective fraction of these amplitudes for the different shells.[17,29] The mean square amplitude was assumed to be linear in the composition.

The multiple-scattering fraction of the measured intensity was calculated following the procedure outlined by Vineyard[35] and Sears.[36] Depending on the wavelength and thickness of the sample, this fraction varies between 3% and 8% of the integral diffuse scattering. Its angular dependence is less than 1% with relation to the total scattering and could be neglected. The isotopic incoherence of the used specimen is negligibly small for the Cu component due to the high purity of the used Cu isotopes; however, for the Ni component it has a value of about 10% of the mean SRO scattering. Therefore this contribution must be corrected for.

For determining the inelastic contributions we made an energy analysis of the scattered neutrons by measuring the time-of-flight spectra for different scattering angles with the time-of-flight spectrometer of the reactor FRJ-2 at the KFA Jülich. The experimental equipment and the procedure of data collection are described in detail by Bauer.[37] The results show that the inelastic contributions are, even for high elastic momentum transfer, of the order of only a few percent of the elastic scattering.

Spin incoherence does not occur in Ni-Cu,[38] and para- and ferromagnetic contributions are negligibly small in comparison to the SRO cross section of the null matrix.[17] After subtracting the background and correcting the unitary transmission and absorption, a least-squares fit of Eq. (5) to the diffuse-scattering data was made, including the above discussed additional scattering contributions and corrections. From this fit we obtain a set of SRO parameters α_i. The fit consisted of a recurring series starting with the SRO parameter of the first shell only and at every step increasing the number of shells by one. In this way the convergence of the fit procedure could be determined. The optimal fit was normally obtained by using 7 or 8 SRO parameters; a still higher number of parameters exceeded the spatial resolution and resulted in nonphysical oscillations in the values of these parameters.

Including the size-effect scattering in Eq. (5) for the least-squares fit, the size-effect parameters β_i,[29] as found already by Vrijen,[21] turned out to be very small, even smaller than the standard deviation of the SRO parameters of the corresponding shells. Therefore the size effect has been neglected in order to keep the number of fitting parameters as low as possible. The small-angle-scattering data, after correction for background, absorption, and detector acceptance, and after calibration with the standard Lupolen data, agreed within the limit of ±10% with the diffuse-scattering data in the region of overlapping κ values.

III. RESULTS

Figure 4 shows two typical diffuse-neutron-scattering patterns of the null matrix, one measured after thermal annealing and the other one after subsequent electron irradiation. At the Bragg positions marked by arrows no indication of Bragg scattering occurs. The solid lines are the least-squares fit of Eq. (5) to the data, using the SRO parameters of the first seven shells. The fit is excellent in the whole recorded diffuse κ range.

The variation of neutron scattering with electron irradiation dose has been investigated in three isothermal irradiation series at different temperatures: (1) irradiation of specimen 1 (thickness: 0.500 mm) at a temperature of 480 K (after a pre-irradiation at 458 K), (2) irradiation of specimen 2 ($d = 0.180$ mm) at 432 K, and (3) of specimen 3 ($d = 0.200$ mm) at 373 K.

Specimen 1 was irradiated with a dose rate of 3.75×10^{13} cm^{-2} s^{-1}. For the irradiation of specimens 2 and 3 a dose rate of 7.00×10^{13} cm^{-2} s^{-1} could be used because of the lower temperature increase due to the lesser thickness. After different irradiation times, both the diffuse neutron scattering and the neutron small-angle scattering were measured, the DNS at the BER II in Berlin, and the SAS at the FRJ-2 of the KFA Jülich. The scattering patterns are shown in Fig. 5 (specimen 1), Fig. 6 (specimen 2), and Fig. 7 (specimen 3) for a κ range between zero and about 1.6 Å^{-1}, each including the pattern recorded after the previous thermal annealing before irradiation. For κ values higher than 1.6 Å^{-1} all curves show a behavior similar to the two examples presented in Fig. 4.

The SRO parameters for the first seven shells, obtained from the least-squares fit of Eq. (5) to all measured diffuse-scattering patterns, are given in Table IV together with their standard deviation. For the fit, the scattering data at κ values below 0.25 Å^{-1} have been excluded to avoid the influence of any long-range interaction on the values of the SRO parameters. For each set of SRO parameters, the corresponding specifications for specimen treatment are also given in Table IV.

After 373-K irradiation, specimen 3 was annealed for 17 h at 480 K for recovery of the excess vacancies from the 373-K irradiation. Subsequently it was irradiated at 480 K. During this post irradiation, for various dose values the small-angle scattering was measured within a κ range of 0.03 Å$^{-1} \leq \kappa \leq 0.50$ Å^{-1}, using special equipment at the multidetector diffractometer of BER II. The scattering patterns are shown in Fig. 8. For reasons of clarity, the data points have been omitted. A typical data set is shown in Fig. 9. After 480-K irradiation, specimen 3 was isochronally annealed

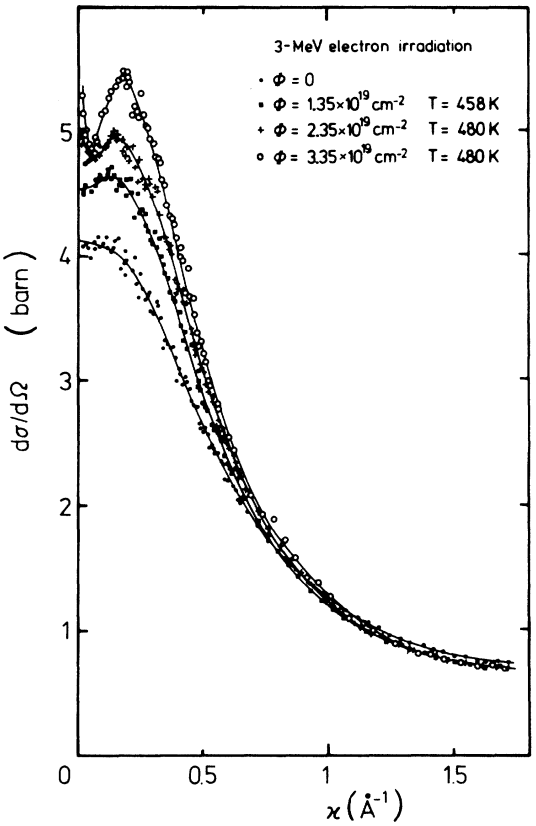

FIG. 5. Neutron small-angle scattering and diffuse SRO scattering of the null matrix, measured after the preparatory thermal treatment (6-h annealing at 870 K and slow furnace cooling) and subsequent isothermal electron irradiation. The SAS data collected at the FRJ-2 extend from $\kappa = 0.01$ Å^{-1} up to $\kappa = 0.22$ Å^{-1}, the diffuse-scattering data obtained at BER II extend from $\kappa = 0.18$ Å^{-1} upwards.

up to 640 K, following with isothermal annealing at 640 K. Figure 9 shows the small-angle-scattering curves which were measured during this annealing treatment.

Specimen 2, previously irradiated at 423 K, was subjected to a similar treatment as specimen 3: it was annealed for 17 h and subsequently post irradiated at 510 K. After annealing and after various irradiation doses, the small-angle scattering was measured at the BER II. The corresponding scattering curves are shown in Fig. 10.

IV. DISCUSSION

Comparison of the SRO parameters in Table IV, derived from measurements after thermal treatment, with the results of other neutron-scattering experiments[17-21] is impeded by the fact that in most cases the heat treatment of the samples is not well defined. A definite heat treatment of the

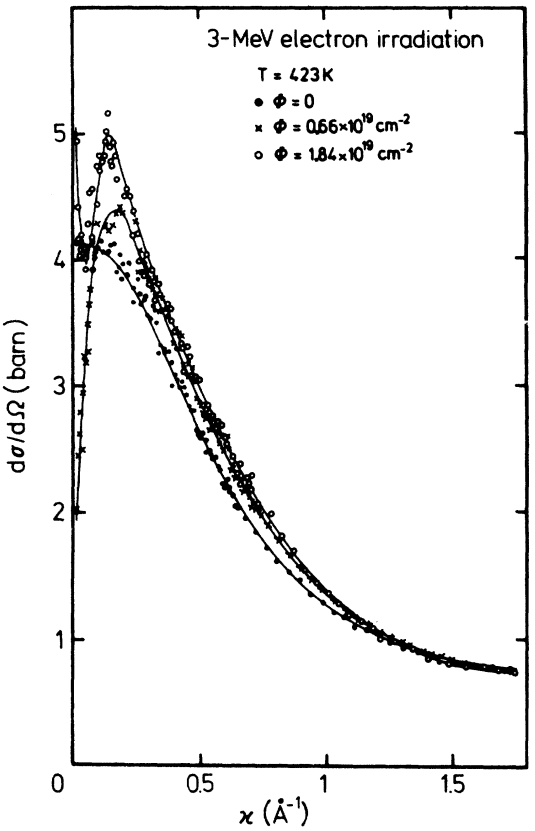

FIG. 6. As for Fig. 5.

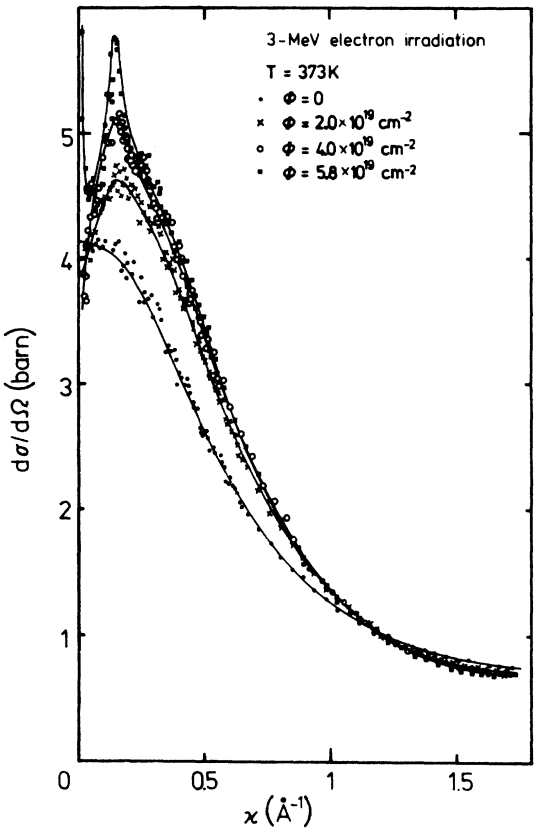

FIG. 7. As for Fig. 5.

specimen was performed by Mozer *et al.*[17] and Vrijen.[21] The main SRO parameter α_1 obtained by Moser agrees very well with our results. The values of α_1 reported by Vrijen are about 10% lower than our values at the corresponding temperatures, but show the same temperature dependence.

After isothermal irradiations at 373, 423, and 458–480 K, a significant increase of the clustering parameters, i.e., an increase of the atomic clustering, was observed. This is in accordance with the assumptions which were made to explain the changes in different physical properties due to irradiation, e.g., electrical resistivity or magnetic susceptibility.[1–16] Moreover, this indicates that radiation-enhanced diffusion provides a sufficient mass transport for increase of short-range clustering. On the other hand, our experiments demonstrate that in specimens which are of suitable dimensions for electron irradiation diffuse neutron scattering can be measured with sufficiently high accuracy to determine the absolute values of the short-range-clustering parameter (standard deviations of α_1 of the order of 3%).

After thermal annealing merely the scattering contribution of short-range clustering is observed in the whole covered κ range, even in the SAS range (Figs. 5–7). However, after irradiation at 373, 423, and 480 K, respectively, quite different SAS patterns are obtained. At κ values between 0.15 and 0.20 Å^{-1}, the monotonic SRO-scattering cross section changes into an intensity maximum associated with a decrease of differential cross section for smaller scattering vectors. It has to be emphasized that this intensity decrease drops below the corresponding SRO cross section obtained by extrapolating the diffuse-scattering data to the SAS region by employing Eq. (5). It even drops below the cross section previously measured after thermal annealing. This effect can be seen clearly in the 423-K irradiation curves (Fig. 6).

The rise of a scattering-intensity maximum in the SAS region in combination with a decrease of scattering intensity at small κ values denotes a coherent modification of the SRO scattering. This behavior can be explained only by a continuous

TABLE IV. All Warren-Cowley SRO parameters for the Ni–41.4-at.%-Cu sample of the present investigation, together with the specifications for specimen treatment. Standard deviations, in units of the last decimal, are given in parentheses.

Spec.	Treatment	T (K)	Dose (10^{19} cm^{-2})	α_1	α_2	α_3	α_4	α_5	α_6	α_7
1	22-h annealing	739[a]		0.132(5)	0.014(9)	0.024(6)	0.024(10)	0.005(7)	−0.010(17)	0.008(5)
2	66-h annealing	690[a]		0.139(6)	0.017(10)	0.027(6)	0.028(6)	0.007(7)	−0.010(18)	0.009(4)
3	66-h annealing	640[a]		0.147(5)	0.019(8)	0.033(5)	0.037(9)	0.012(6)	−0.012(15)	0.017(4)
1	6-h annealing	870[b]	0	0.149(4)	−0.013(7)	0.022(4)	0.025(8)	−0.004(6)	0.001(14)	0.004(4)
1	irradiation	458	0.15	0.169(4)	−0.006(8)	0.032(5)	0.021(9)	0.001(7)	−0.001(16)	0.005(4)
1	irradiation	458	1.25	0.191(4)	0.017(8)	0.043(5)	0.035(9)	0.005(7)	0.005(16)	0.009(4)
1	irradiation	480	2.25	0.200(4)	0.020(8)	0.049(5)	0.035(10)	0.008(8)	0.010(18)	0.012(5)
1	irradiation	480	3.25	0.206(6)	0.029(10)	0.052(6)	0.044(12)	0.010(9)	0.003(21)	0.016(6)
3	6-h annealing	870[b]	0	0.150(4)	−0.001(7)	0.033(5)	0.026(8)	0.005(6)	0.002(15)	0.009(4)
3	irradiation	563	1.00	0.161(4)	0.018(7)	0.037(4)	0.029(8)	0.009(6)	0.003(14)	0.010(4)
3	irradiation	373	3.00	0.201(5)	0.012(9)	0.045(6)	0.028(10)	0.005(8)	0.007(18)	0.007(5)
3	irradiation	373	5.00	0.214(6)	0.009(10)	0.050(7)	0.028(12)	0.003(9)	0.012(21)	0.008(6)
3	irradiation	373	6.76	0.218(7)	0.007(13)	0.053(8)	0.025(15)	0.005(11)	0.023(26)	0.006(7)
2	6-h annealing	870[b]	0	0.150(4)	−0.001(7)	0.036(4)	0.019(7)	0.005(6)	0.010(13)	0.007(4)
2	irradiation	423	0.66	0.183(5)	0.008(10)	0.034(6)	0.031(11)	0.006(9)	−0.004(20)	0.007(6)
2	irradiation	423	1.84	0.202(7)	0.001(14)	0.045(8)	0.018(14)	0.005(10)	0.013(26)	0.007(7)

[a] Fast cooling.

[b] Slow furnace cooling.

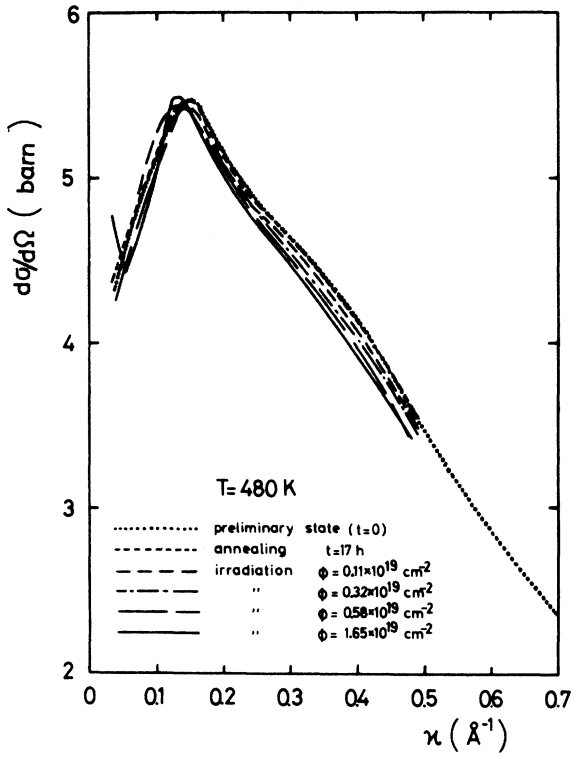

FIG. 8. Neutron SAS patterns measured at BER II after annealing and subsequent post irradiation at 480 K. The preliminary state was obtained by isothermal irradiation at 373 K (see Fig. 6). For reasons of clarity, the data points have been omitted. A typical data set is shown in Fig. 9.

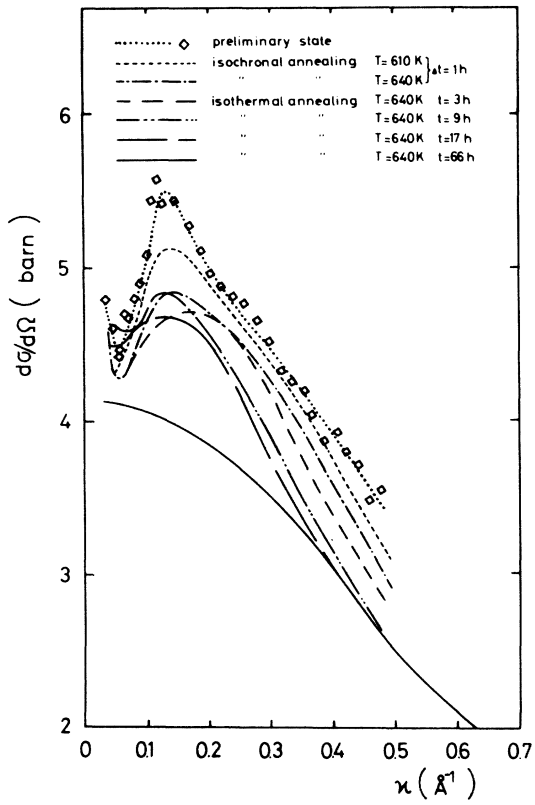

FIG. 9. Neutron SAS patterns measured at BER II during isochronal and isothermal annealing treatment. The preliminary state is that obtained by the post irradiation at 480 K (Fig. 8).

rearrangement of the existing SRO structure. Any segregation or clustering which might develop without rearranging the existing SRO structure would have led to an incoherent superposition of its scattering contribution to the SRO scattering.

Short-range clustering in a binary alloy means the existence of randomly distributed small regions enriched in one or the other component. The coherent modification of the SRO scattering indicates a correlation between these enriched regions, leading to an arrangement of the regions with preferential distances between one another. The average cluster-cluster distance is correlated to the position of the intensity maximum; it is of the order of about 25 Å. An ordering of the enriched regions according to preferential distances is equivalent to the formation of periodic concentration fluctuations. The peak intensity increases with increasing irradiation dose. At 423 and 373 K the shape of the peak sharpens during irradiation and shifts smoothly to smaller κ values as is expected for a spinodal decomposition.[39-41]

For some scattering patterns, the intensity increases again at κ values below 0.04 $Å^{-1}$, indicating another small-angle-scattering contribution which possibly is due to an incoherent segregation. This additional SAS contribution could not be studied in detail because of the limited scattering-intensity rates at these low κ values.

Detailed conclusions derived from the results of the present paper will be presented in two following papers.[22,23] In particular the influence of short-range clustering on the residual electrical resistivity will be treated by means of the theoretical model of Rossiter and Wells,[42] and the temperature dependence of short-range clustering under irradiation will be discussed. Further-

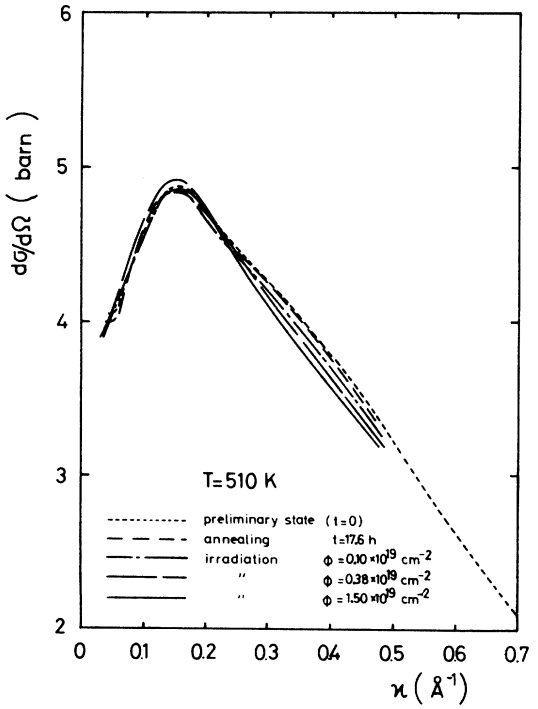

FIG. 10. Neutron SAS patterns analogous to those shown in Fig. 8, here after annealing and post irradiation at 510 K. The preliminary state is that obtained by isothermal irradiation at 423 K (see Fig. 6).

more, a comparison of the observed concentration fluctuations with the theoretical models of spinodal decomposition will be given and the limits of the critical temperature will be discussed, taking into consideration the SAS pattern of the post-irradiation experiments. Finally, the mechanism of radiation-enhanced diffusion and the effect of irradiation on phase stability in Ni-Cu will be discussed.

ACKNOWLEDGMENTS

The authors are very grateful to Dr. habil. J. Schelten, KFA Jülich for making available the SAS instrumentation of FRJ-2, for assistance during the SAS-data collection, and for valuable discussions. We are indebted to Dr. G. S. Bauer, KFA Jülich, for assistance in measuring the time-of-flight spectra. We wish to thank Dr. J. Jakschik, Physikalisch-Technische Bundesanstalt (P.T.B.), Institut Berlin, and technicians for their help during the irradiation experiments. The authors are obliged to Dr. H. Wollenberger for helpful discussions and suggestions and for encouraging criticism of the manuscript. We also wish to thank the staff of the HMI groups *C*1 and *C*2 for their technical assistance.

[1]W. Köster and W. Schüle, Z. Metallkd. 48, 592 (1957).
[2]J. L. Meijering, Acta Metall. 5, 257 (1957).
[3]F. M. Ryan, E. W. Pugh, and R. Smoluchowski, Phys. Rev. 116, 1106 (1959).
[4]W. Schüle and H. P. Kehrer, Z. Metallkd. 52, 168 (1961).
[5]A. Ascoli, *Radiation Damage in Solids* (IAEA, Vienna, 1962), pp. 105–112.
[6]A. Kussmann and H. Wollenberger, Z. Metallkd. 54, 521 (1963).
[7]A. Ascoli, M. G. Belloni, and G. T. Queriolo, Phys. Lett. 9, 305 (1964).
[8]W. Schüle, B. C. Kelley, M. S. Wechsler, and J. M. Williams, Oak Ridge National Laboratory, Report No. ORNL-3676 (1964).
[9]G. M. Schwab and F. v. Stutterheim, Z. Naturforsch. 24A, 1607 (1969).
[10]R. Burger and J. Auer, Z. Naturforsch. 23A, 2125 (1968).
[11]S. Takamura and S. Okuda, Radiat. Eff. 17, 151 (1973).
[12]R. Poerschke, Jülich Report, Report No. Jül FF 1100 (unpublished).
[13]R. Poerschke and H. Wollenberger, Radiat. Eff. 24, 217 (1975).
[14]R. Poerschke and H. Wollenberger, Proceedings of an International Conference at Gatlinburg, Tennessee, Report No. CONF-751006-P2, 1975 (unpublished).
[15]R. Poerschke and H. Wollenberger, J. Phys. F 6, 27 (1976).
[16]R. Poerschke, U. Theis, and H. Wollenberger, J. Phys. F 10, 67 (1980).
[17]B. Mozer, D. T. Keating, and S. C. Moss, Phys. Rev 175, 868 (1968).
[18]J. W. Cable, E. O. Wollan, and H. R. Child, Phys. Rev. Lett. 22, 1256 (1969).
[19]A. T. Aldred, B. D. Rainford, T. J. Hicks, and J. S. Kouvel, Phys. Rev. B 7, 218 (1973).
[20]R. A. Medina and J. W. Cable, Phys. Rev. B 15, 1539 (1977).
[21]J. Vrijen and S. Radelaar, Phys. Rev. B 17, 409 (1978).
[22]W. Wagner, R. Poerschke, and H. Wollenberger (unpublished).
[23]R. Poerschke, W. Wagner, and H. Wollenberger (unpublished).
[24]R. Sizmann, J. Nucl. Mater. 69–70, 386 (1978).
[25]G. Moliere, Z. Naturforsch. 3A, 78 (1948).
[26]W. Heidrich, Jülich Report No. Jül-1006-FF (unpublished).
[27]J. Wurm, Jülich Report No. Jül-587-FN (unpublished).
[28]R. Poerschke and H. Wollenberger, J. Nucl. Mater. 74, 48 (1978).
[29]B. E. Warren, *X-Ray Diffraction* (Addison-Wesley, Reading, Mass., (1969).

[30]A. Axmann, M. Bischoff, R. Kind, M. Kubitz, M. Müllerburg, J. L. Pollet, and V. Tschammer (unpublished).
[31]A. Axmann (unpublished).
[32]J. Schelten, Habilitationsschrift, Ruhr-Universität Bochum, 1977 (unpublished).
[33]W. Schmatz, T. Springer, J. Schelten, and K. Ibel, J. Appl. Crystallogr. 7, 96 (1974).
[34]F. Lihl, H. Ebel, and W. Baumgartner, Z. Metallkd. 62, 42 (1971).
[35]G. H. Vineyard, Phys. Rev. 96, 93 (1954).
[36]V. F. Sears, Adv. Phys. 24, 1 (1975).
[37]G. S. Bauer, Jülich Report No. Jül.-1158-FF (unpublished).
[38]S. F. Mughabghab and D. I. Garber, *Neutron Cross Sections, Vol. 1, Resonance Parameters* (BNL Report No. 325, Brookhaven, 1973).
[39]J. W. Cahn, Trans. AIME 242, 166 (1968).
[40]J. S. Langer, in *Fluctuations, Instabilities and Phase Transitions*, edited by T. Riste (Plenum, New York, 1975), p. 19.
[41]K. Binder, C. Billotet, and P. Mirold, Z. Phys. B30, 183 (1978).
[42]P. L. Rossiter and P. Wells, J. Phys. C 4, 354 (1971).